Review of applications to laser accelerators in vacuum

Contents

- Introduction

- Approach and milestones
  - Far field interaction, no matter in interaction volume
  - Gaussian laser beams, providing most strong fields
  - Acceleration by longitudinal electric field components
  - Acceleration based on using transverse fields
  - Diffractive dominated IFELs

- Acceleration by fundamental Gaussian mode
  - Laser fields for Gaussian TEM_{00} mode
  - Resonator with holes for particle beam non collinear with laser beam axis
  - Phase synchronization improvement for α_{opt}
  - Acceleration field profiles E_α for different γ, P, z_R, λ_s
  - Acceleration rate as a function of P and γ for $\lambda_s\gamma^2 > z_R$
  - Comments on particle beam qualities requirements

- Vacuum laser acceleration with axicon
  - Axicon focus fields
  - Structure of the longitudinal electric fields in axicon axis
  - Acceleration rate, comparison with noncollinear Gaussian beam scheme

- IFEL in Gaussian beam
  - IFEL equations for γ, ψ in adiabatic approximation for all field parameters
  - Limitation from radiation losses at high energies

- IFEL in Gaussian beam, small z_f
  - Analytical equations for γ, ψ in $r_\perp=0$ approximation

- IFEL project of UCLA – Kurchatov Institute
  - Non adiabatically tapered undulator for IFEL experiment at UCLA
  - Numerical simulations
  - Schematic construction of double tapered undulator
  - Magnetic fields and trapped electron trajectories
  - Synchronization curves and energies of accelerated electron
  - Sensitivity to laser beam jitter
  - Depending on laser beam power
  - Fraction of trapped particles
  - Output beam from IFEL accelerator

- Laser acceleration staging and prebunching problem
  - General approach
  - Transverse beam bunching by laser field
  - Principally new prebunching scheme

IFEL experiments

IFELA: Wernick & Marshall 1992 ***(PRA 46, 3566)***

- First proof-of-principle IFEL experiment
- 5 MW at $\lambda = 1.6$ mm, gradient 0.7 MV/m, gain 0.2 MeV

BNL-IFEL: Van Steenbergen, Gallardo et al. 1996 ***(PRL 77, 2690)***

- Microbunching observed 1998 ***(PRL 80 4418)***
- 1-2 GW at $\lambda = 10.6$ μm, gradient 2.5 MV/m, gain 1 MeV

MIFELA: Yoder, Marshall, Hirshfield 2001 ***(PRL 86, 1765)***

- All electrons accelerated, phase dependency of the acceleration
- 6 MW at $\lambda = 10$ cm, gradient 0.43 MV/m, gain 0.35 MeV

STELLA: Kimura et al. 2001 ***(~~to be~~ published, AAC proceedings)*** 2000

- First staging of two IFEL modules. (Phys. Rev. Spec. Top. 4, 101301, 20
- 0.1-0.5 GW at $\lambda = 10.6$ μm, gain up to 2 MeV

STELLA 2

- 5 GW $\lambda = 10,6$ μm gain ~ 4 MeV. AAC, 2002
  $\Delta W/W = 12\%$

Laser fields for Gaussian fundamental TEM_{00} mode.

$$\vec{E} = E_x \vec{e}_x + E_z \vec{e}_z \qquad \vec{B} = B_y \vec{e}_y + B_z \vec{e}_z$$

$$E_x = E_0 \frac{e^{-\frac{x^2+y^2}{w(z)^2 w_0^2}}}{w(z)} \cdot \sin\left(kz - \omega t + \varphi_0 + \frac{k\left(x^2+y^2\right)}{2R(z)} - \operatorname{arctg}\frac{z}{z_R} \right)$$

$$E_z = E_0 \frac{e^{-\frac{x^2+y^2}{w(z)^2 w_0^2}}}{k \cdot w(z)^2 \cdot w_0^2} \cdot 2x \cdot \cos\left(kz - \omega t + \varphi_0 + \frac{k\left(x^2+y^2\right)}{2R(z)} - 2 \cdot \operatorname{arctg}\frac{z}{z_R} \right)$$

$$B_y = B_0 \frac{e^{-\frac{x^2+y^2}{w(z)^2 w_0^2}}}{w(z)} \cdot \sin\left(kz - \omega t + \varphi_0 + \frac{k\left(x^2+y^2\right)}{2R(z)} - \operatorname{arctg}\frac{z}{z_R} \right)$$

$$B_z = B_0 \frac{e^{-\frac{x^2+y^2}{w(z)^2 w_0^2}}}{k \cdot w(z)^2 \cdot w_0^2} \cdot 2y \cdot \cos\left(kz - \omega t + \varphi_0 + \frac{k\left(x^2+y^2\right)}{2R(z)} - 2 \cdot \operatorname{arctg}\frac{z}{z_R} \right)$$

where

$$k = \frac{2\pi}{\lambda}; \qquad z_R = \frac{k w_0^2}{2}; \qquad w(z)^2 = 1 + \frac{z^2}{z_R^2}; \qquad R(z) = z + \frac{z_R}{z}$$

w_0 – radius of the field E waist; z_R – Rayleigh length

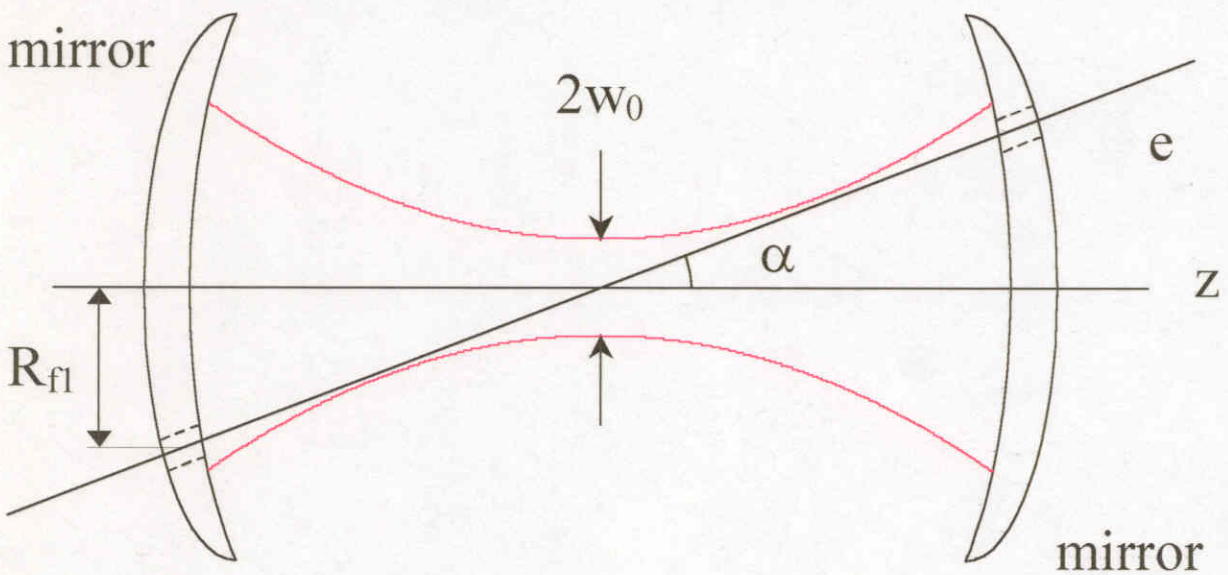

Phase synchronization improvement

For particle crossing the resonator at angle α

$$\delta\varphi = \frac{2\pi}{\lambda} z \frac{1+\alpha^2\gamma^2}{2\gamma^2}$$ - phase slippage with respect to a plane wave

$$\varphi_1 = \frac{k\left(x^2+y^2\right)}{2R_z} - \operatorname{arctg}\frac{z}{z_R}$$ - additional phase of Gaussian mode

$\varphi_1-\delta\varphi$ - relative phase seeng by particle, can be more smooth due to $k(x^2+y^2)/2R_z$ term.

$$\alpha_{opt} \cong \frac{1}{2}\sqrt{\frac{\lambda_s}{2z_R}}$$

z_R=0.18 m, γ=150 $\lambda\gamma^2>z_R$

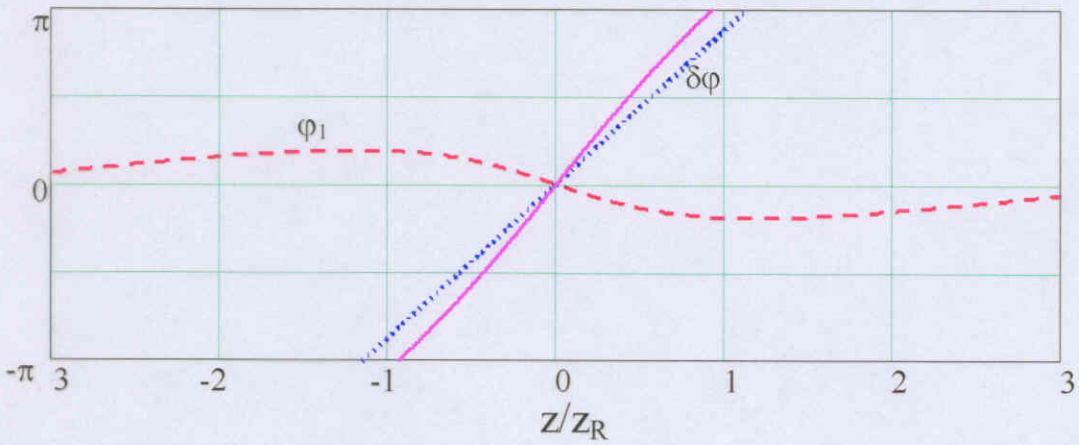

z_R= 0.03 m, γ=1000 $\lambda\gamma^2>z_R$

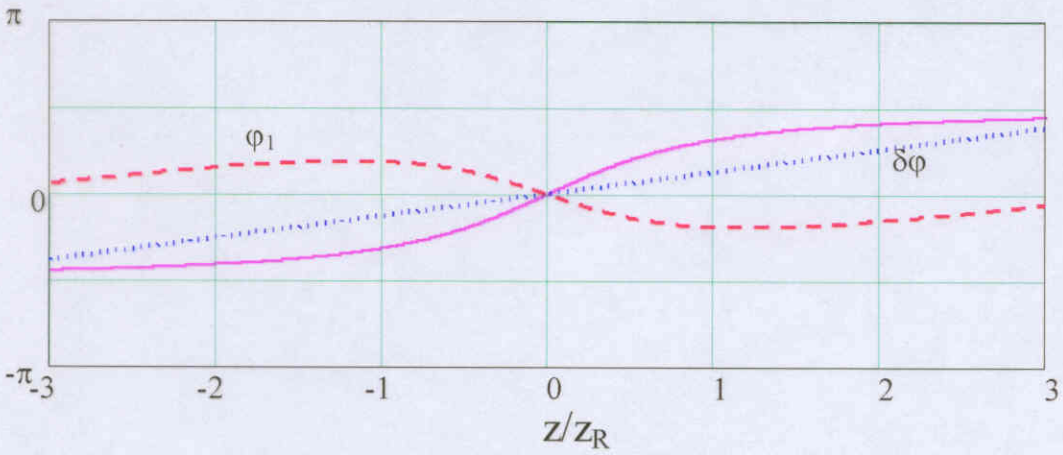

Accelerating field profiles E_α in Gaussian beam

Noncollinearity angle $\alpha_{opt} = \frac{1}{2}\sqrt{\frac{\lambda_s}{2z_R}}$

Initial particle phase $\varphi_0=\pi/2$

Wavelength $\lambda s=10.6$ μm

Laser beam power $P=10^{13}$ W

Rayleigh length $z_R=0.03$ m

Particle energy $E_p=\gamma\, m_p c^2$

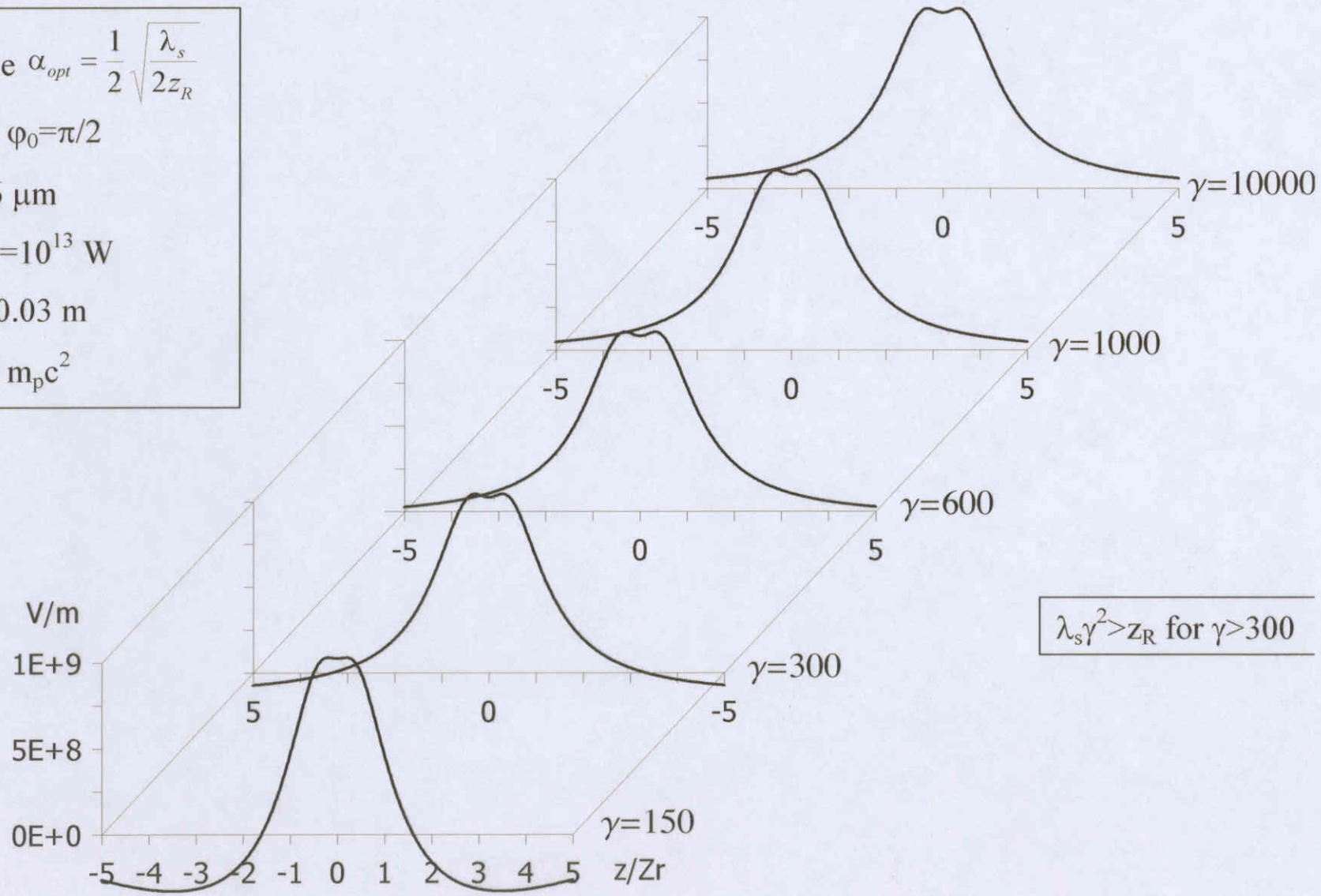

$\lambda_s\gamma^2 > z_R$ for $\gamma > 300$

The shapes are similar to that for $z_R=0.18$ with 6 times higher peak fields.

Accelerating field profiles E_α in Gaussian beam

Noncollinearity angle $\alpha_{opt} = \frac{1}{2}\sqrt{\frac{\lambda_s}{2z_R}}$

Initial particle phase $\varphi_0=\pi/2$

Wavelength $\lambda_s=10.6$ μm

Laser beam power $P=10^{13}$ W

Rayleigh length $z_R=0.18$ m

Particle energy $E_p=\gamma\, m_p c^2$

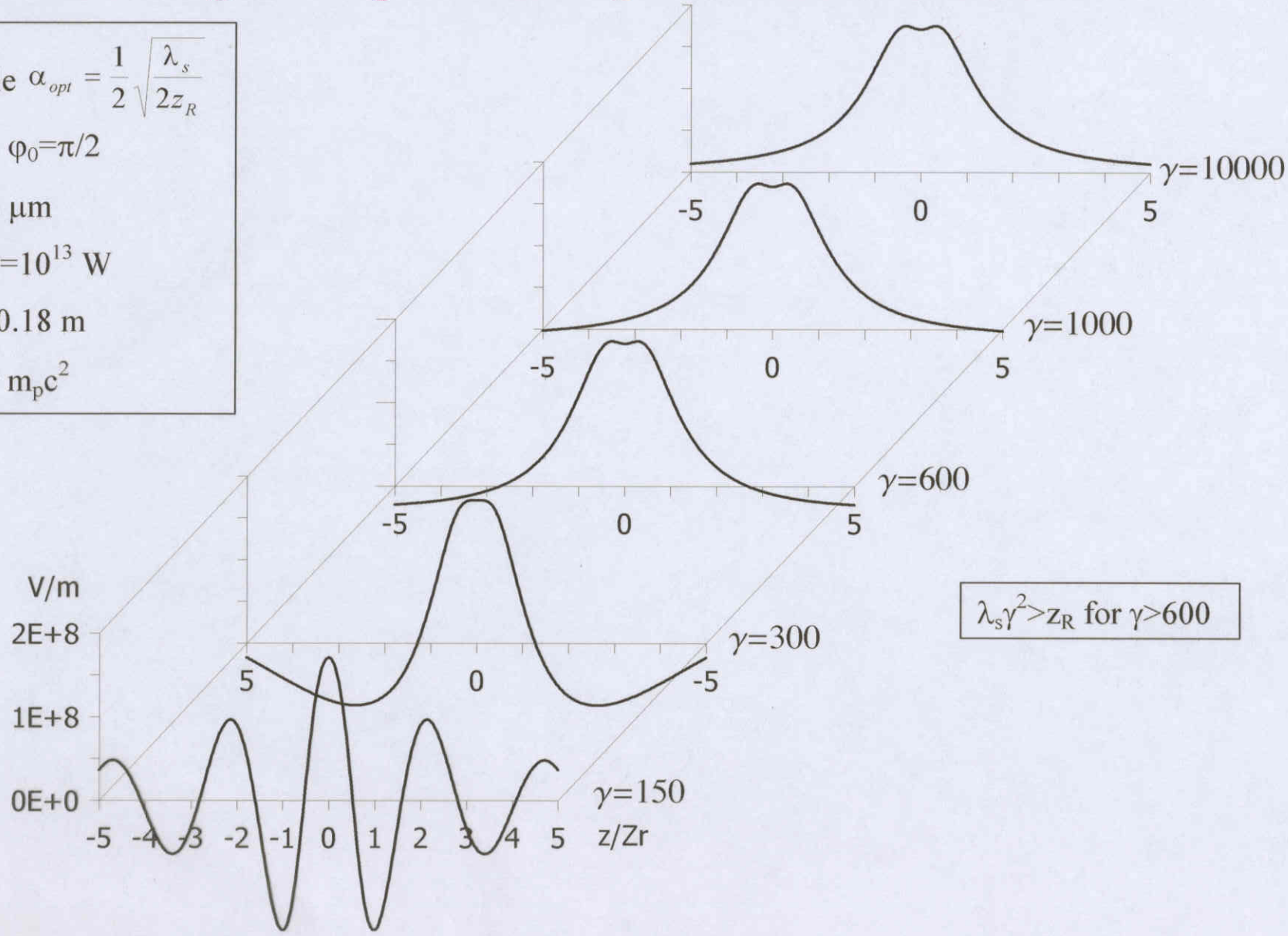

$\lambda_s\gamma^2 > z_R$ for $\gamma>600$

For $\gamma>600$ acceleration is positive in wide range $-2z_R \div 2z_R$.

Profile shapes are not dependent on γ (at $\gamma>600$) and on laser power P.

Acceleration rate in Gaussian beam as a function of particle energy.

Laser beam power $P=10^{13}$ W - red line
$P=10^{12}$ W - blue line
Rayleigh length $z_R=0.03$ m - solid line
$z_R=0.18$ m - dashed line
Noncollinearity $\alpha=\alpha_{opt}$

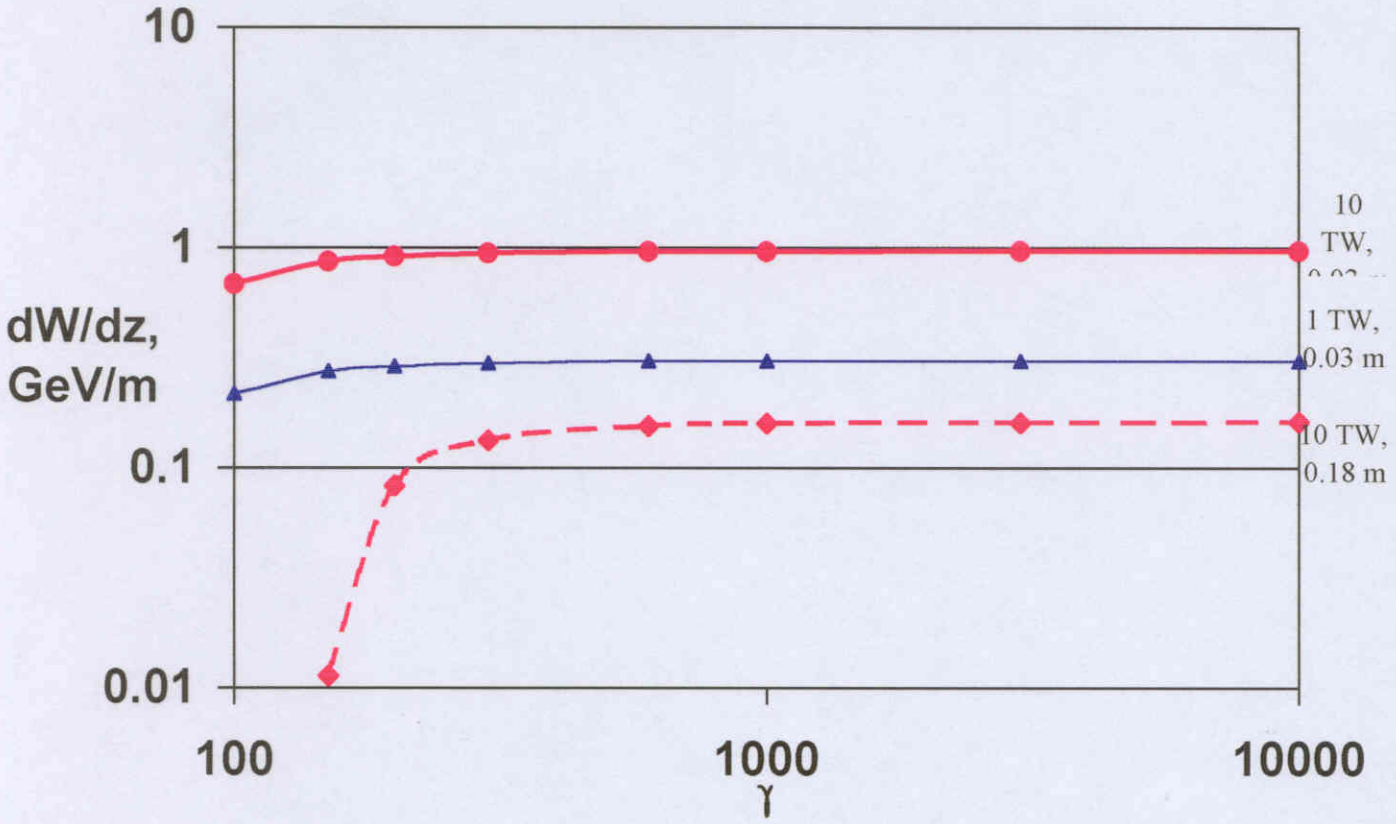

For $\gamma>300$ the following relation is valid:

$$\frac{dW}{dz}\left(\frac{eV}{m}\right)=9.15\cdot\frac{\sqrt{P(W)}}{z_R(m)}$$

Acceleration rate in Gaussian beam as a function of the laser beam power P

Particle energy $\gamma=10^3$

Rayleigh length $z_R=0.03$ m - solid line

$z_R=0.18$ m - dashed line

Noncollinearity $\alpha=\alpha_{opt}$

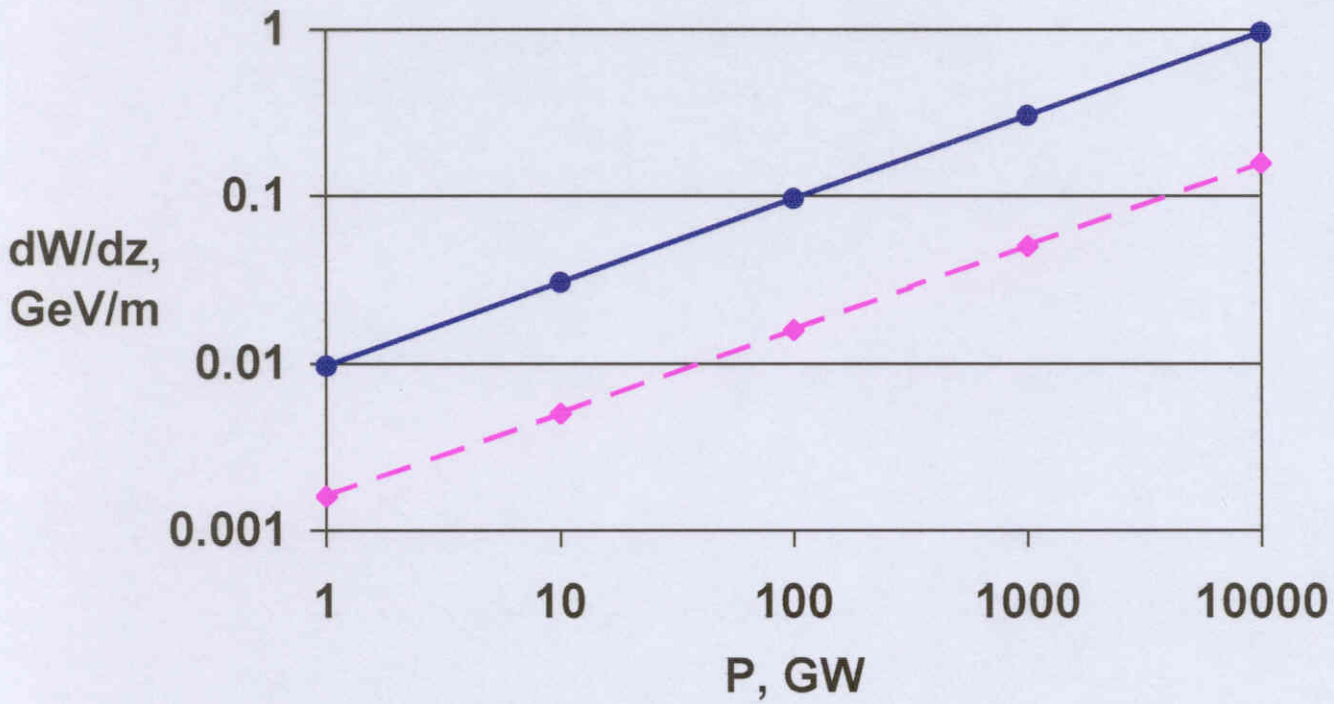

$$\frac{dW}{dz}\left(\frac{eV}{m}\right)=9.15\cdot\frac{\sqrt{P(W)}}{z_R(m)}$$

Relation is valid in wide range of power P.

Comment on particle beam quality requirements

- For ε_n=1 mm mrad the acceleration gain per one section is $\Delta W/W=0.01$

- Focusing and crossing angle α
  - For $\alpha=1/\gamma$ laser field induce no net transverse deviation of particle in vicinity of the focus

$$e\left(E_0\cos\alpha-\frac{v}{c}H_0\right)\cong 0$$

  - Acceleration and beam focusing are correlated

    $\alpha>1/\gamma$ perfect acceleration along with focusing deacceleration along with defocusing.

    $\alpha<1/\gamma$ correlation is opposite: acceleration is accompanying by defocusing
  - $\alpha=\alpha_{opt}$, $\gamma=10^3$ acceleration and focusing take place simultaneously.

- Acceleration rate as a function of initial particle phase φ

  $\Delta\varphi=0$ $dW/dz=(dW/dz)_{max}$

  $\Delta\varphi=\pm\pi/2$ $dW/dz=0$

  $\Delta\varphi=0\div\pi/2$ slope, feed back possible for beam stability

- Multiple section acceleration, possibilities for tuning
  - Intersection phase shifts
  - Intersection crossing angle correction and dispersion
  - Small transverse displacements of laser beam lines in sections stability and beam acceptances

Vacuum laser acceleration with axicon

- Axicon laser beam

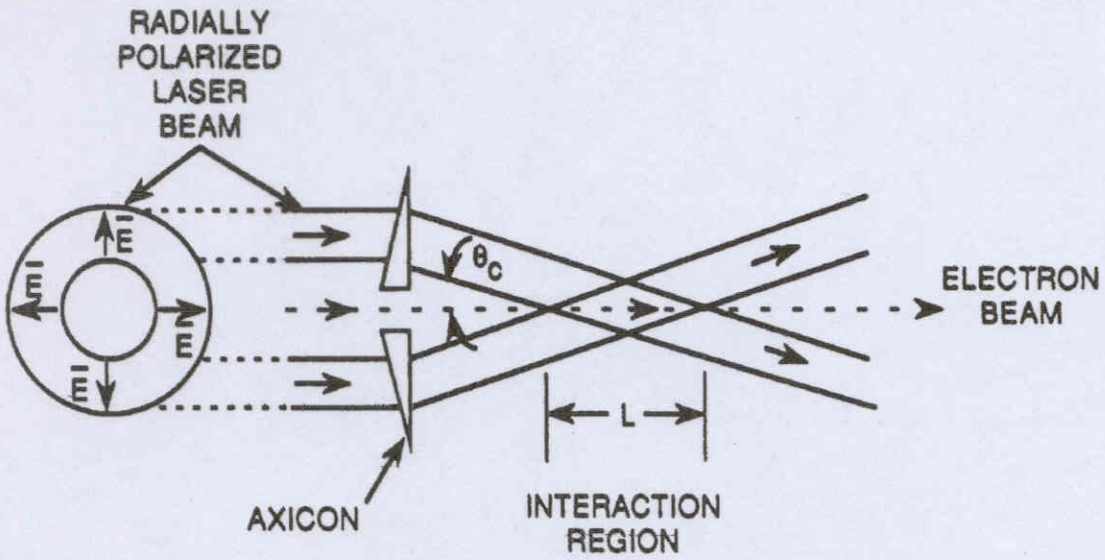

- Schematic of optical system and termination of interaction

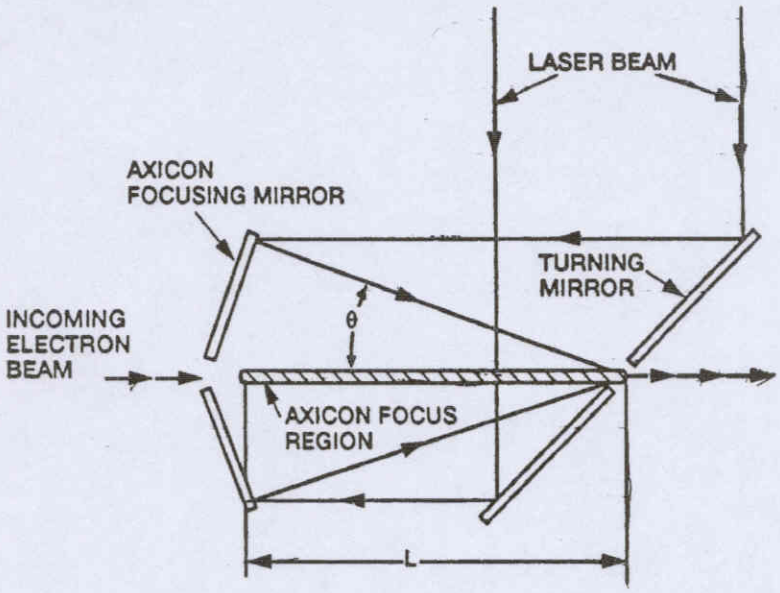

- Special properties
  - Radially-polarized axisymmetric electric field
  - Line axicon focus with pure longitudinal field E_z on Z axis
  - Limited interaction length L_{int} (for nonzero net accelaration)

Axicon focus field

- Field on the of the focus (z axis)

$$E_z(0,z,t) = E_0\theta \frac{2\sqrt{e\theta ka}}{\left[\frac{z}{L} + i\theta ka\right]^2} Q(\xi)\exp\left[i(\omega t - kz) + i\frac{\pi}{2}\right]$$

where

$$Q(\xi) = 1 + \xi^2 + \sqrt{\pi}\xi\left(\frac{3}{2} + \xi^2\right)e^{\xi^2}\left[1 + erf(\xi)\right];$$

$$\xi = ika\left[\frac{z/L}{2(z/L + ik\theta a)}\right]^{\frac{1}{2}}$$

- Structure of the longitudinal electric field along z-axis at r=0

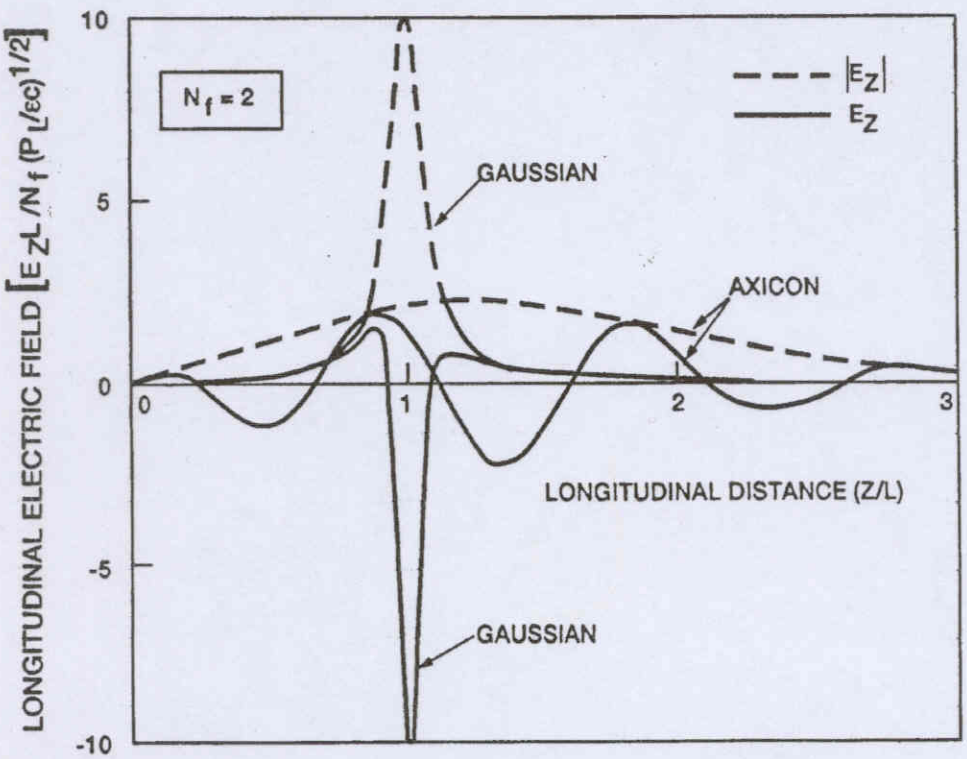

- The factor exp[i(ωt-kz)] is dropped
- L_{int}=L contains some peaks,

$$z_R = L/2\pi N_f$$

- Longitudinal electric field structure for an axicon focus with two different Fresnel numbers

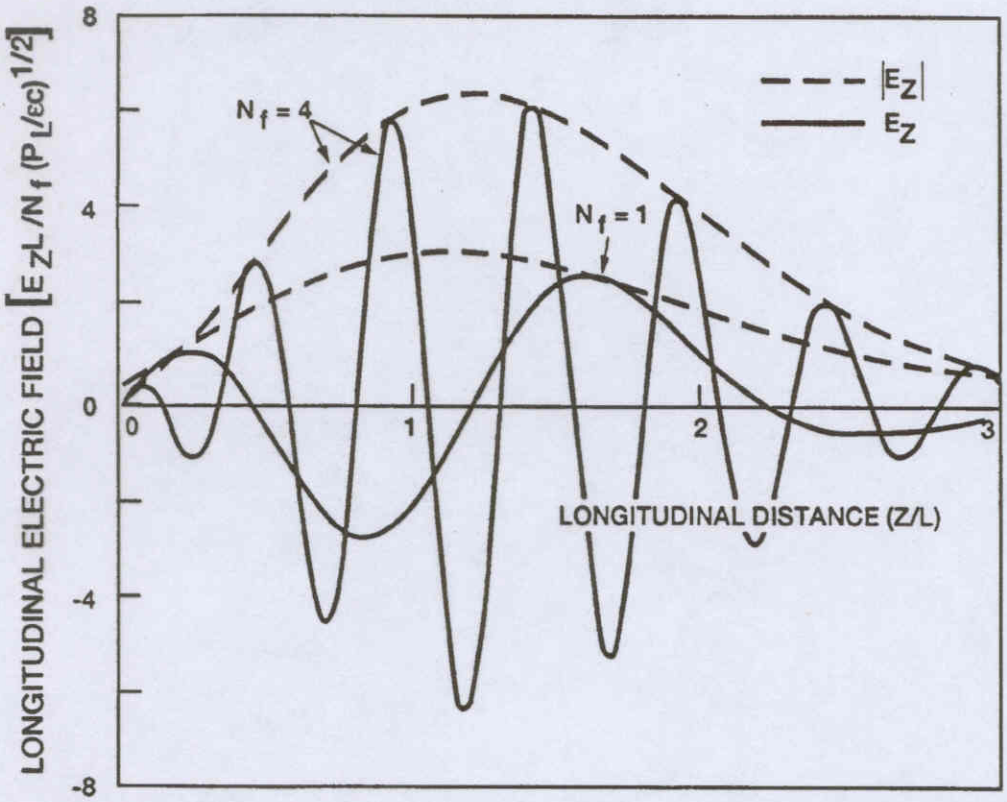

The factor exp[i(ωt-kz)] is dropped. Oscillation comes from field complex amlitude structure mainly, the fact that rays cross the axis at angle θ

$$\Delta\varphi = \frac{2\pi\Delta z}{2\lambda_s\gamma^2/\left(1+\theta^2\right)} \cong \frac{2\pi}{\lambda_s}\cdot\frac{\Delta z\theta^2}{2};$$

- $z_{eff}=L/N_f$ caused by finite $\theta>>1/\gamma$
  $z_R=L/2\pi N_f$ takes into account phase of the focused wave (not plane wave)

- Acceleration rate achievable with axicon.
  - $E_{z\,max}=(E_0/ka)\cdot N_f^{3/2}$;
  - $\left\langle \frac{dW}{dz} \right\rangle = q(E_{z\,max})\cdot \frac{\Delta z_{eff}}{2L} = 5.94\left[\frac{P_L \lambda \theta}{a^3}\right]^{1/2} \frac{eV}{m}$

  - Tendency

    Larger θ gives larger $E_{z\,max}$ but smaller $\Delta z_{eff}=L/N_f$.
    (It is actually less if the wave phase is taken into account more correctly).

- Comparision
  - Axicon (C. Steinhauer, W. Kimura, J. of Appl. Phys. 72, 3237, 1992)

P_L	Crossing angle	λ	$4a$	L_{int}	dW/dz
W	mrad	μm	cm	cm	MeV/m
10^{13}	100	10.6	1	5	155
10^{13}	100	10.6	0.4	2	612

  - Gaussian mode

P_L	Crossing angle	λ	Waist w_0	$L_{int}=2z_R$	dW/dz
W	mrad	μm	cm	cm	MeV/m
10^{13}	6.6	10.6	0.03	6	1200

- Gaussian mode provides twice higher acceleration rate with the same laser power on comparable path length.
  Smooth phase channel (small crossing angles) provides single isolated peak of the field

IFEL in Gaussian beams

- Accelerator equations for planar wiggler, strong laser fields, plane wave approximation

$$\frac{d\gamma}{dz} = \frac{eE_0}{2mc^2}\cdot\frac{k}{\gamma}[J_0(G)-J_1(G)]\sin\psi + \frac{eE_0}{2mc^2}\frac{K_L}{\gamma}\sin 2k_w z -$$

$$-\frac{2}{3}r_e\gamma^2 k_w^2\left\{\frac{K^2}{2}+\frac{K_L^2}{2}+K_L K[J_0(G)+J_1(G)]\cos\psi-\frac{K^2+K_L^2}{2}\cos 2k_w z\right\}$$

$$\frac{d\psi}{dz} = k_w - k_s\frac{1}{2\gamma^2}\left\{1+\frac{K^2}{2}+\frac{K_L^2}{2}+K_L K[J_0(G)-J_0(G)]\cos\psi\right\}$$

Here

$$G(z)=\frac{k_s}{k_w}\cdot\frac{K^2+K_L^2}{8\gamma^2};\quad K=\frac{eB_{w0}}{mc^2k_w};\quad K_L=\frac{eE_0}{mc^2k_s};\quad k_s=\frac{\omega}{c};\quad k_w=\frac{2\pi}{\lambda_w};$$

$$\psi(z)=\int_0^z k_w dz - k_s\int_0^z\frac{dz}{2\gamma^2}\left\{1+\frac{K^2}{2}+\frac{K_L^2}{2}+K_L K[J_0(G)-J_0(G)]\cos\psi\right\}-\psi_0$$

J_0, J_1 – Bessel functions

- Adiabatic approximation

Small changing of parameters $k_w(z)$, $K(z)$, $K_L(z)$, $E_0(z)$, $G(z)$, $B_{0w}(z)$ on one period $2\pi/k_w$.

Laser field is not necessary small, $K_L \neq 0$.

Radiation losses limit the net acceleration to zero at high energies $\gamma > 10^6$.

- Plane wave and adiabatic approaches are not adequate for real performances.
- Beam emittance required

$\beta > \lambda_s\gamma^2$ $\quad$ $\varepsilon_n < 0.1\cdot\lambda_s\gamma$

$z_R > \lambda_s\gamma^2$ $\quad$ $\sigma = 0.1\cdot w_0^2$

Maximum acceleration rate in a collinear IFEL for a field of 10^{11} V/m and λ_s=1 μm (solid line) and synchrotron-radiation energy losses per unit length in a bending-magnet field 5 T (dashed line)

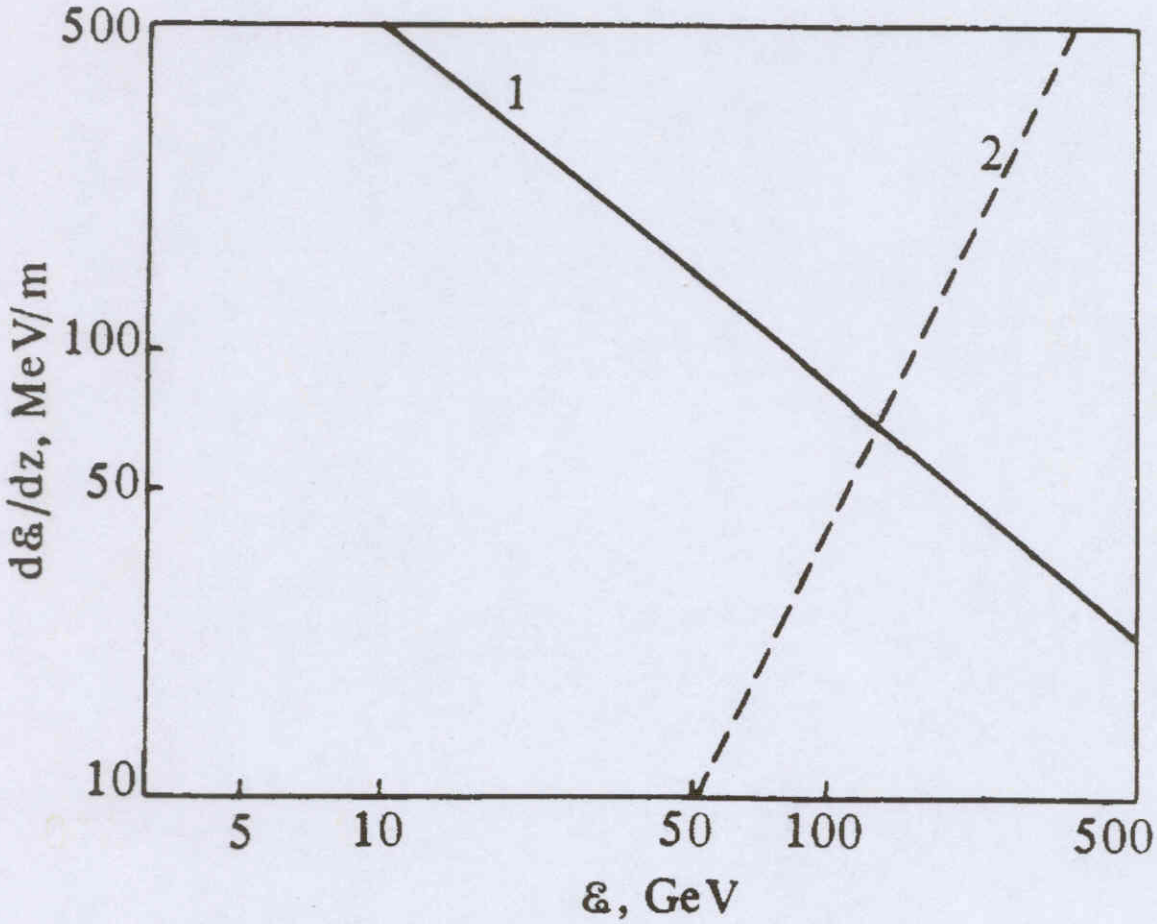

IFEL in Gaussian beam, small z_R

- Analytical equations for Gaussian mode with diffraction in 1D approach ($\sigma_\perp$=0)

$$\frac{d\gamma}{dz} = \frac{eE_0}{2mc^2}\cdot\frac{k}{\gamma}[J_0(G)-J_1(G)]\frac{\sin\psi}{\left(1-\frac{z^2}{z_R^2}\right)^{\frac{1}{2}}} + \frac{eE_0}{mc^2}\frac{K_L}{\gamma}\sin 2k_w z\frac{1}{\left(1-\frac{z^2}{z_R^2}\right)^{\frac{1}{2}}};$$

$$\frac{d\psi}{dz} = k_w - k_s\frac{1}{2\gamma^2}\left\{1+\frac{K^2}{2}+\frac{K_L^2}{2}+K_L K[J_0(G)-J_0(G)]\cos\psi+\gamma^2\theta^2\right\} - \frac{1}{z_R\left(1+\frac{z^2}{z_R^2}\right)^{\frac{1}{2}}};$$

Approximation $r_\perp$=0 is not valid for focus region

- Conclusion

More correct consideration of Gaussian mode field and optimization k(z) parameters for real performance numerical simulations are needed with using equations of motions and 3D field maps of both laser and undulator.

Inverse Free Electron Laser Project
UCLA – Kurchatov Institute

Non-adiabatic, diffraction dominated regime

- Powerfull (Twatt) CO_2 laser (most powerfull used for IFELs)
- Gaussian mode, short Rayleigh range, 3.6 cm, small focal waist 0.35 mm
- Short accelerator length, 50 cm
- Focal region is also using for acceleration

- Initial electron energy 14 MeV
- Normalized e.b. emittance 10 mm·mrad
- Charge 0.3 nC; pulse length 3 ps

Extraordinary characteristics

- High electron acceleration gain, 41 MeV
- High percentage of accelerated electrons, >20%

Neptune beamline

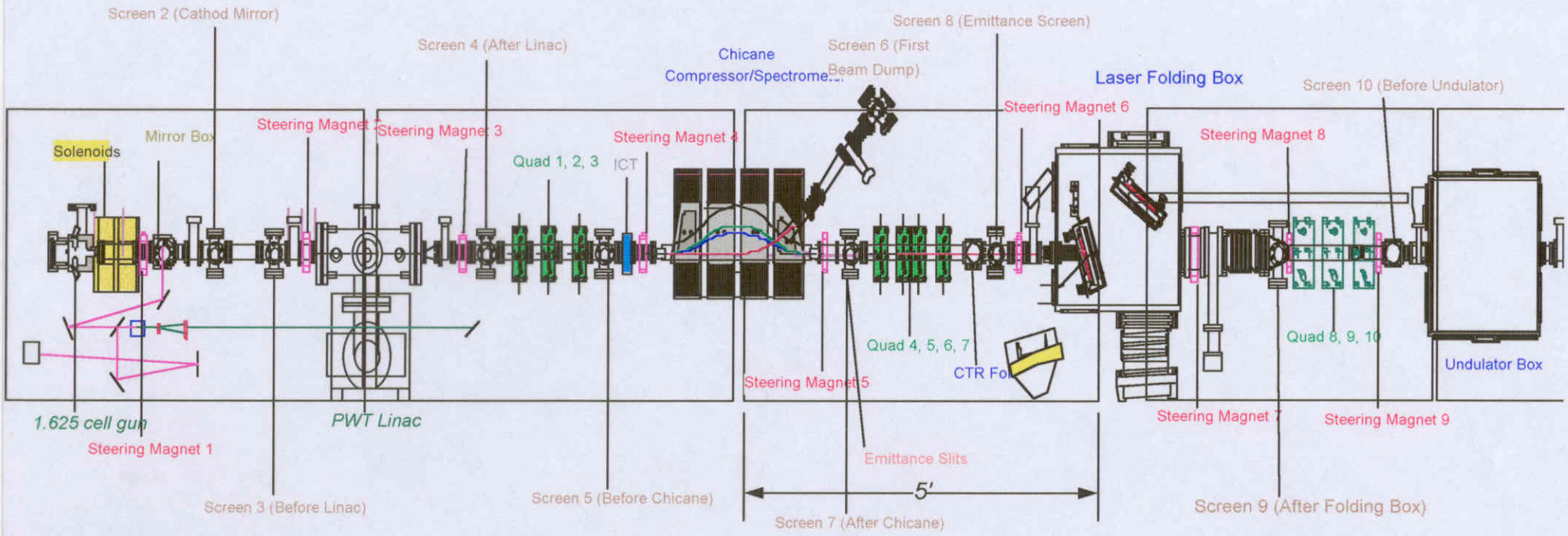

Non adiabatically tapered undulator for IFEL experiment at UCLA

- Basic parameters of IFEL for the undulator construction.
  - Laser wavelength 10.6 μm
    Laser power P 0.4 – 0.8 TW
    Rayleigh length z_R 3.6 cm
    Laser beam waist w_0 0.35 mm
    Laser beam size at the undulator entrance ww_0 2.5 mm

  - Initial electron energy W_0 14 MeV
    E. b. emittance ε_n 10 mm mrad
    E. b. rms radius at focus 0.15 mm
    E. b. rms radius at the undulator entrance 0.50 mm
    Total acceleration length 50 cm
    Total acceleration gain 40 MeV
- Basic undulator requirement
  - Transparency to laser and electron beams
  - Strong fields with strong tapering of both $\lambda_w(z)$ and $B_w(z)$
  - Optimized acceleration in Gaussian mode including focus area.

Numerical simulation procedure and magnet construction optimization

- Codes
  - Radia code for 3D magnetic field maps
  - Lorenz equation code with MathCAD for reference electron trajectory
  - 3D code TREDI, IFEL version 2
    (Lienard Wiechert potential approach)

- Successive approximations
  - Reference electron trajectory, analysis of synchronizations
  - Corrections of the field
  - Correction limit 0.1%

- Optimization goal
  - Synchronism with the laser field
  - Maximum acceleration rate
  - Maximum acceptance (capture and acceleration of an electron bunch)
  - Small sensitivity to laser jitter

Schematic construction of planar hybrid undulator for IFEL project

Blue – p.m. blocks
Red – poles
Brown – side magnets
Gray – correction frame

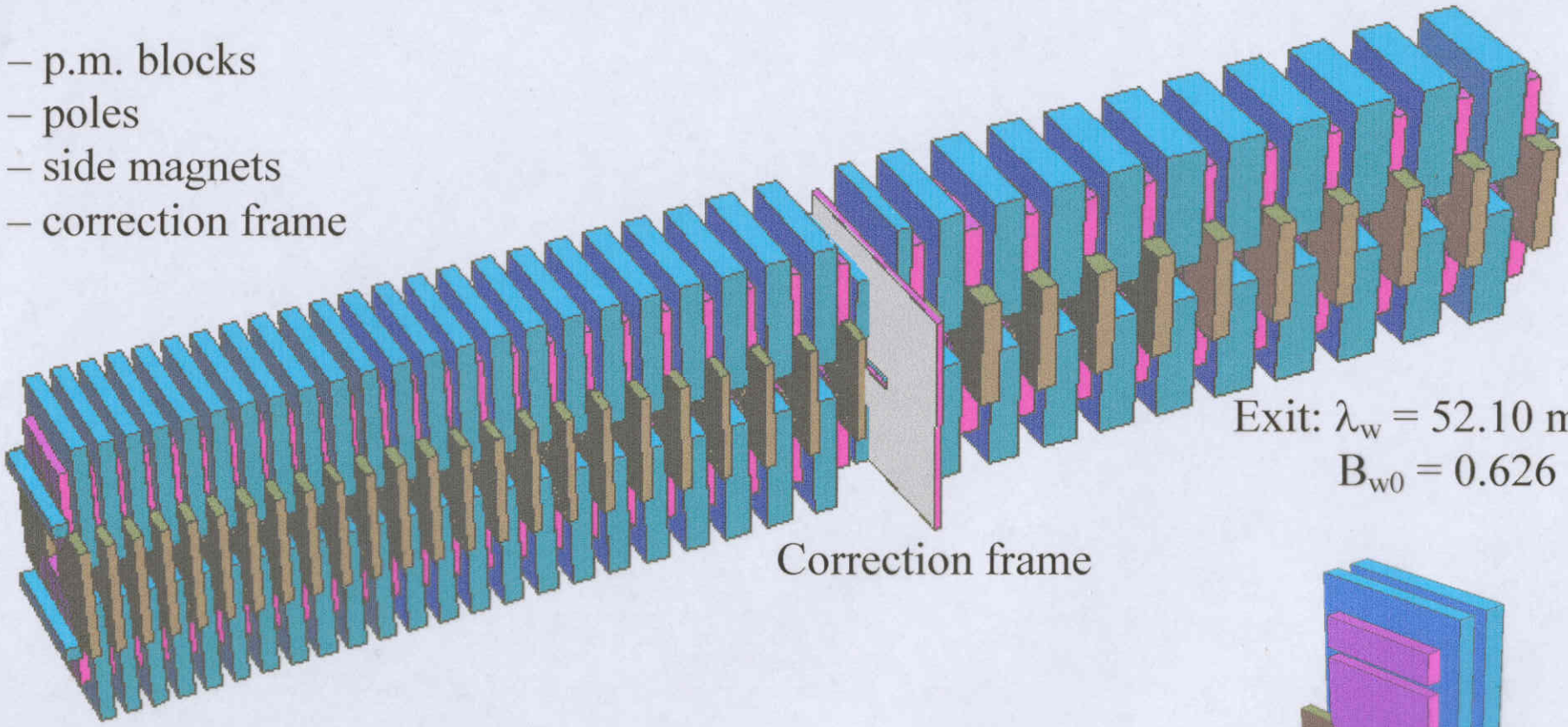

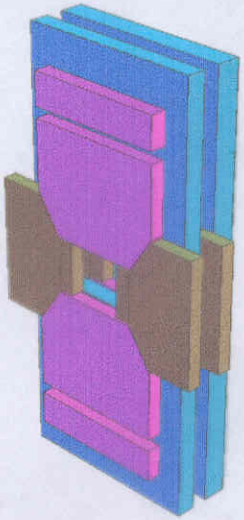

Magnet cell

ЗА.000.000

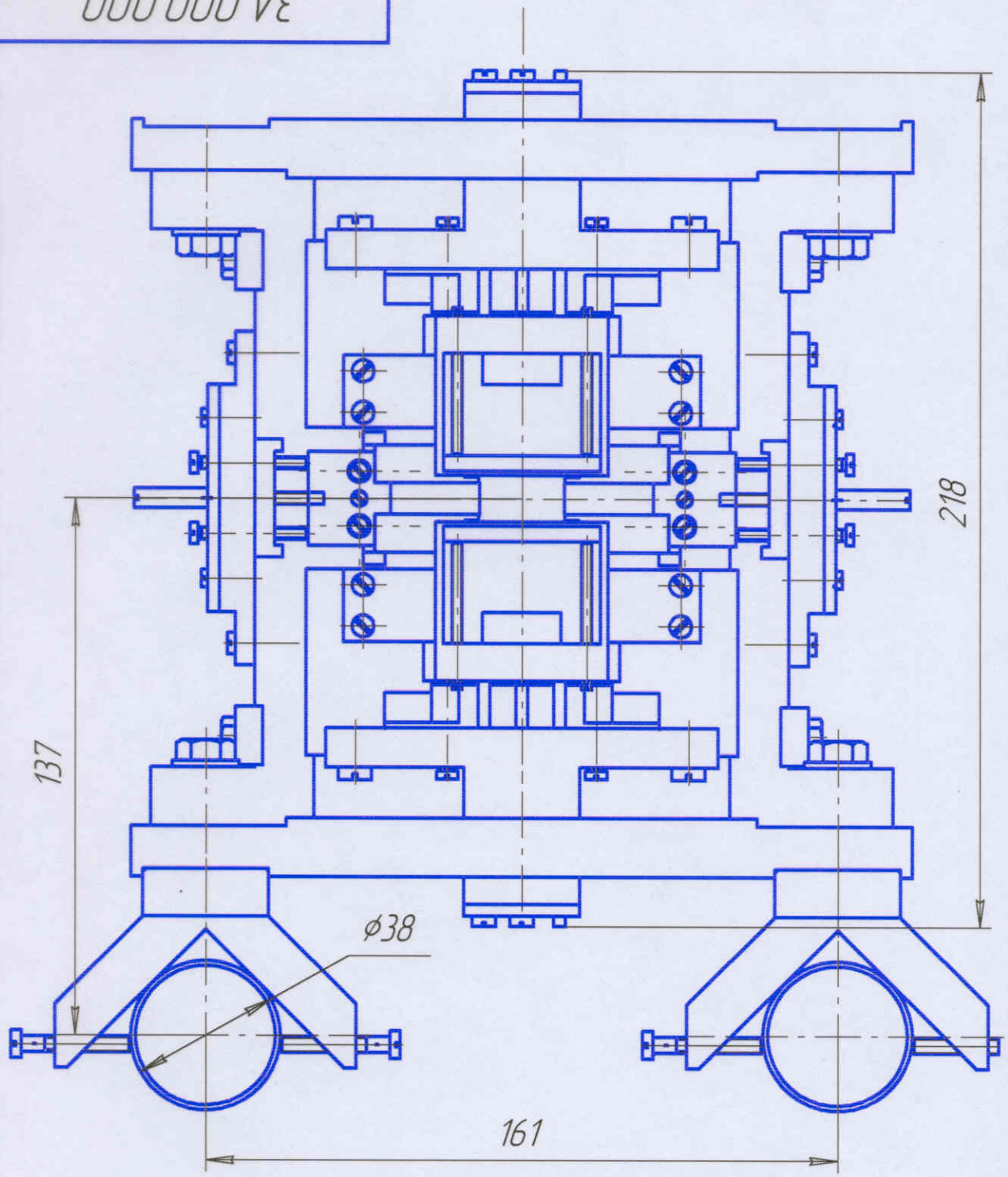

Перв. примен.

Справ. №

Подп. и дата

Инв. № дубл.

Взам. инв. №

Подп. и дата

Инв. № подл.

Изм.	Лист	№ докум.	Подп.	Дата
Разраб.				
Пров.				
Т.контр.				
Н.контр.				
Утв.				

ЗА.000.000

Undulator
for Neptune Lab.

Лит.	Масса	Масштаб
Лист	Листов	

RRC Kurchatov Institute

Копировал

Формат А4

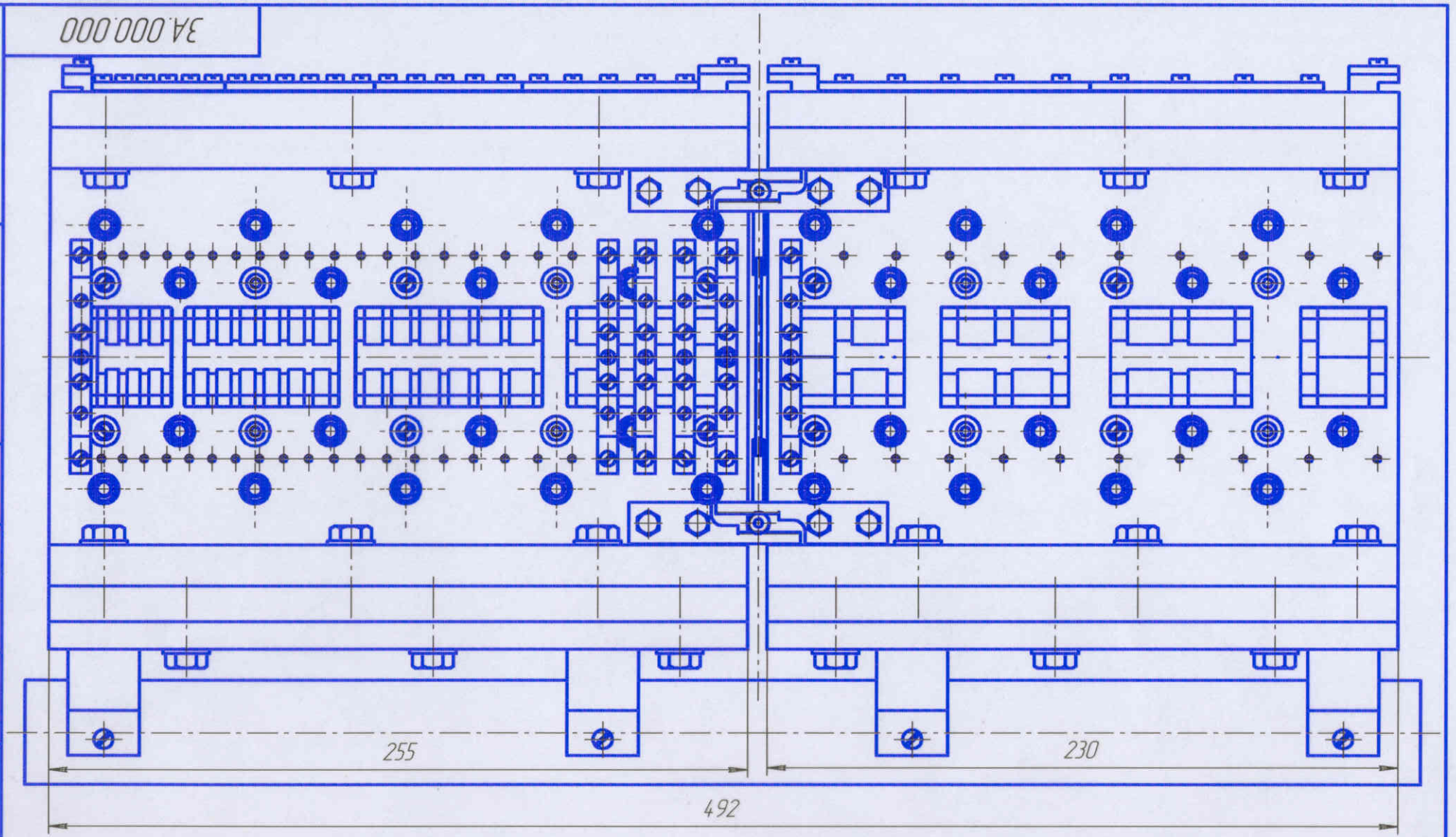

					3A.000.000	
Изм.	Лист	№ докум.	Подп.	Дата	Undulator for Neptune Lab.	Лит. / Масса / Масштаб
Разраб.						
Пров.						Лист / Листов
Т.контр.						
Н.контр.					RRC Kurchatov Institute	
Утв.						

Копировал

Формат А3

Перв. примен.

Справ. №

Подп. и дата

Инв. № дубл.

Взам. инв. №

Подп. и дата

Инв. № подл.

Magnetic fields (a) and trapped electron trajectories (b) in the undulator

Option A

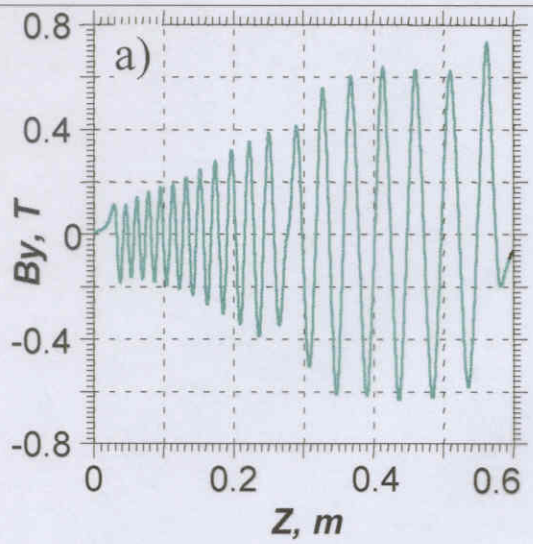

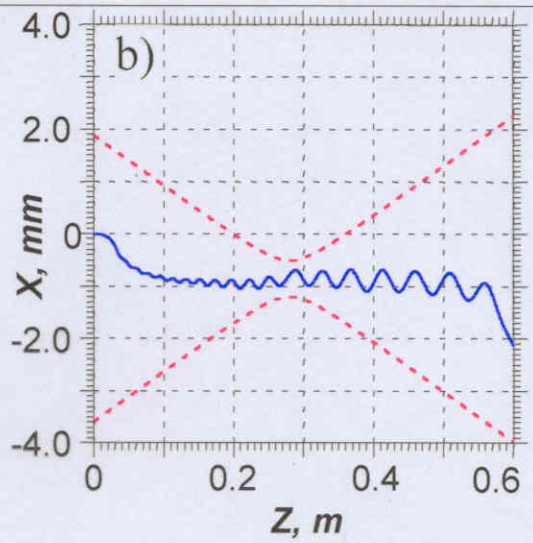

Option B

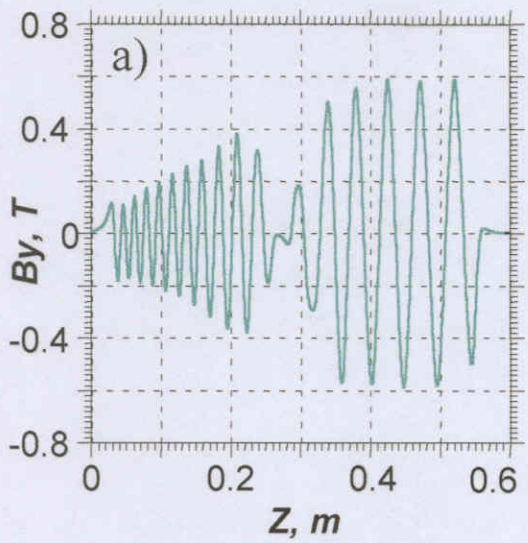

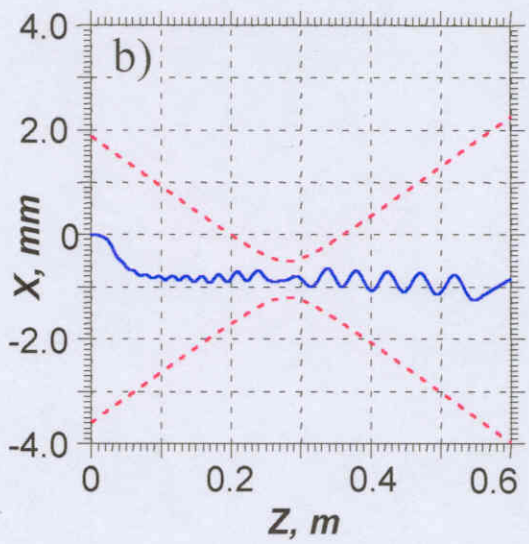

Option C

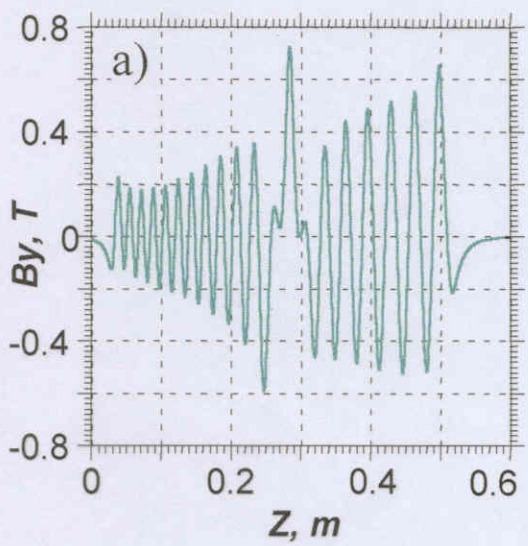

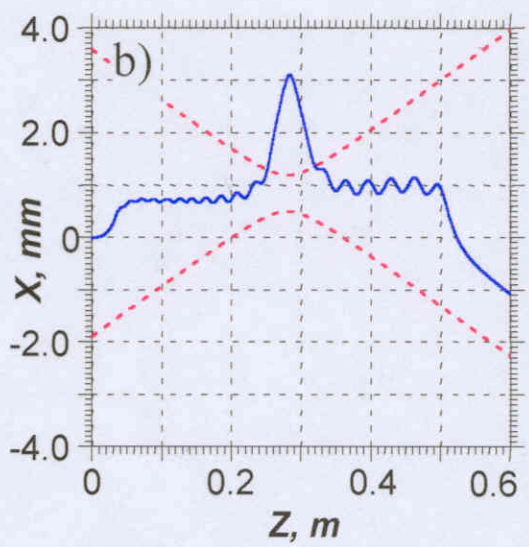

Synchronization curves and energies of accelerated electron

Option A

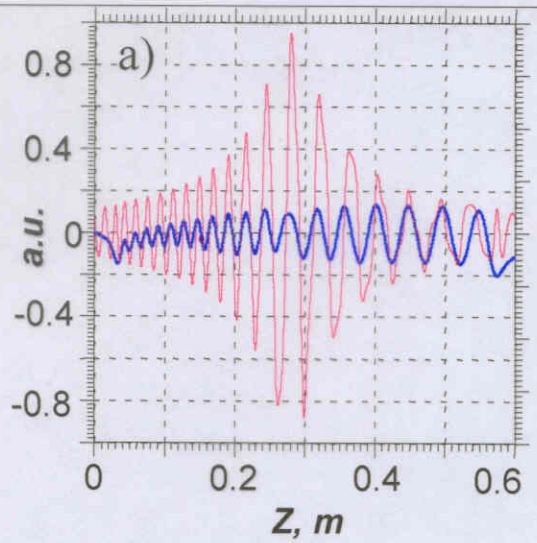

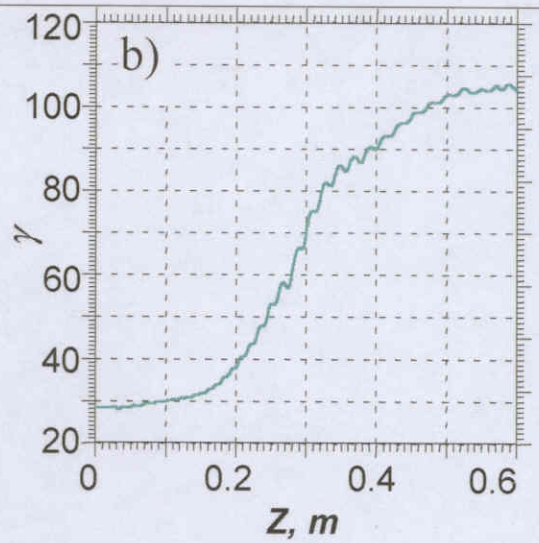

Option B

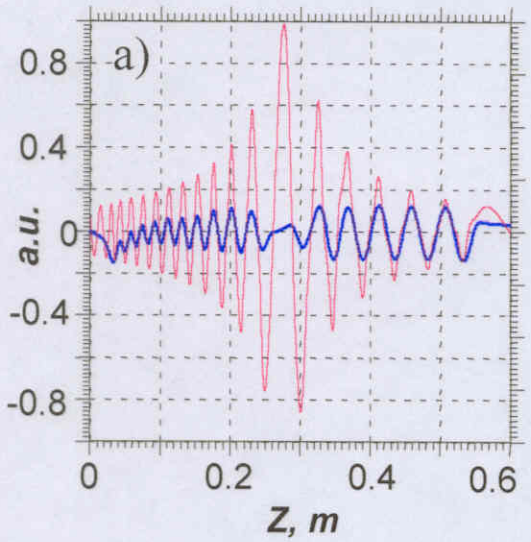

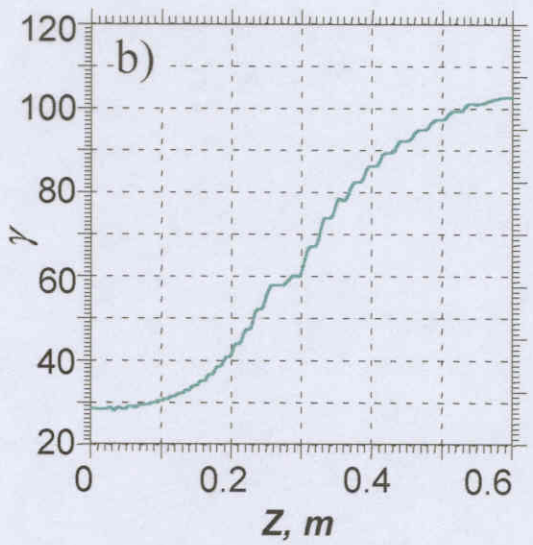

Option C

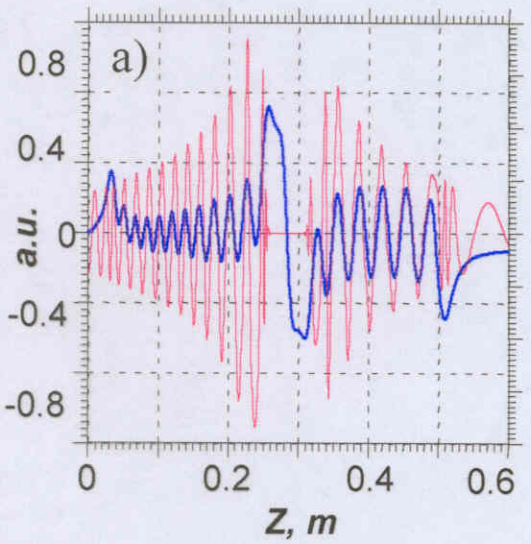

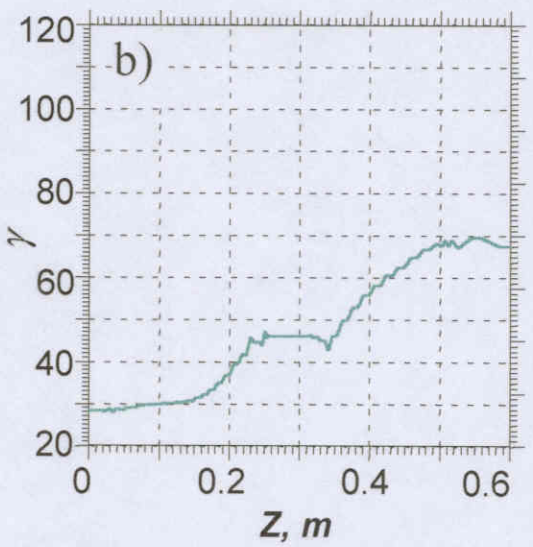

On the left: thin red line – laser field seen by electron
solid blue line – transverse velocity of the electron
On the right: accelerated electron energies along z.

• Sensitivity to laser beam jitter

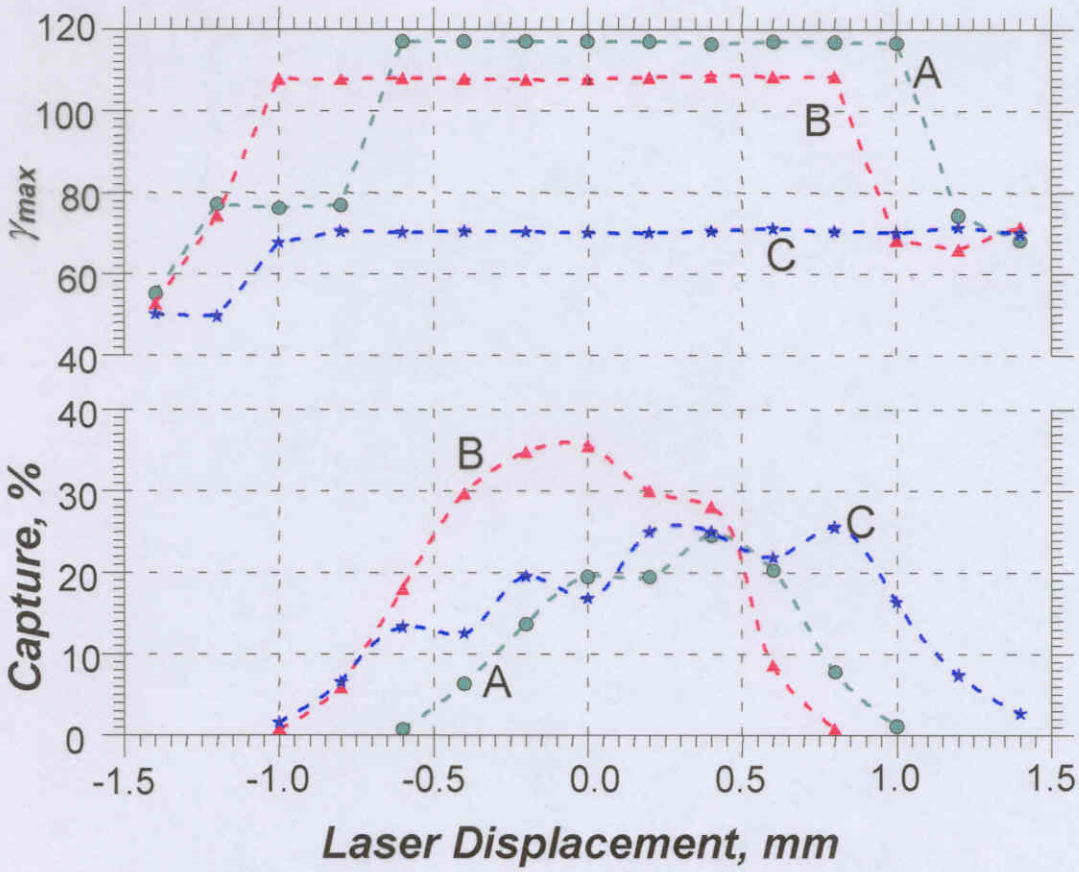

The higher γ_{max} the more sensitivity to jitter.
Displacement ± 0.25 mm can be acceptable.
Option A was chosen for construction.

• Dependence on laser power

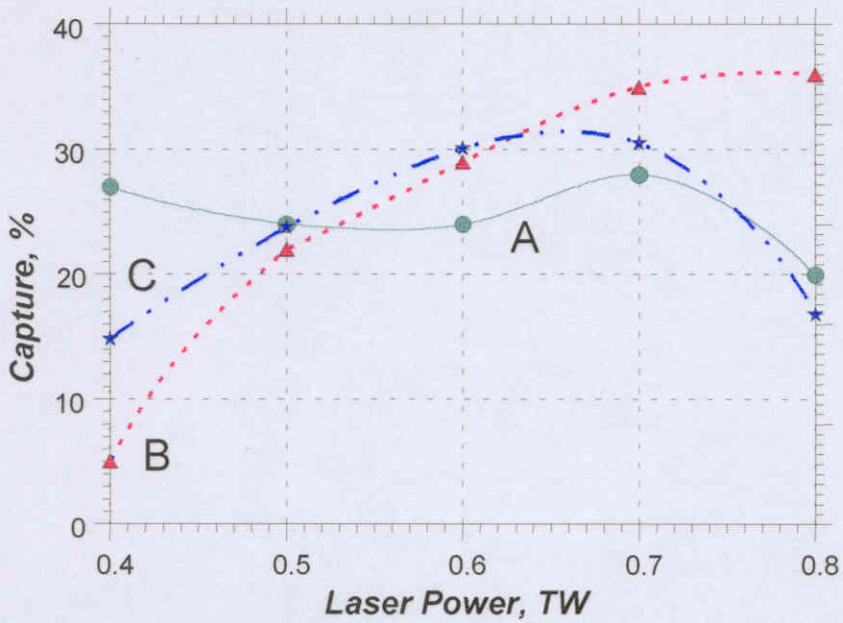

Capture ~ 25% in wide range of P.
The higher γ ... the less capture fraction at P > 0.5 TW

- **Fraction of trapped particles when laser beam properties are changed.**

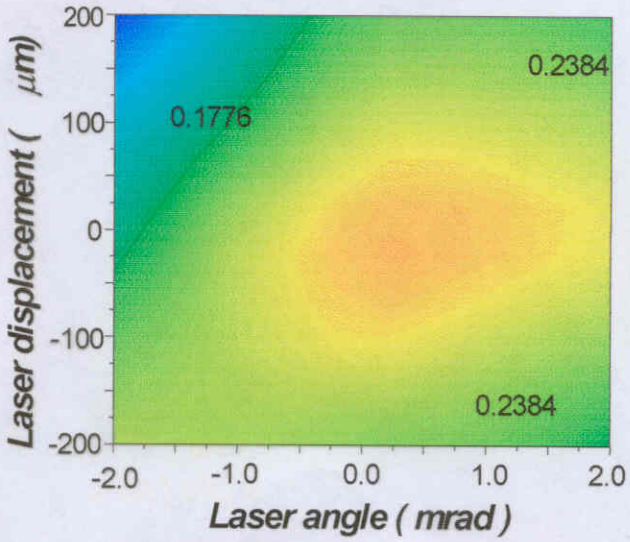

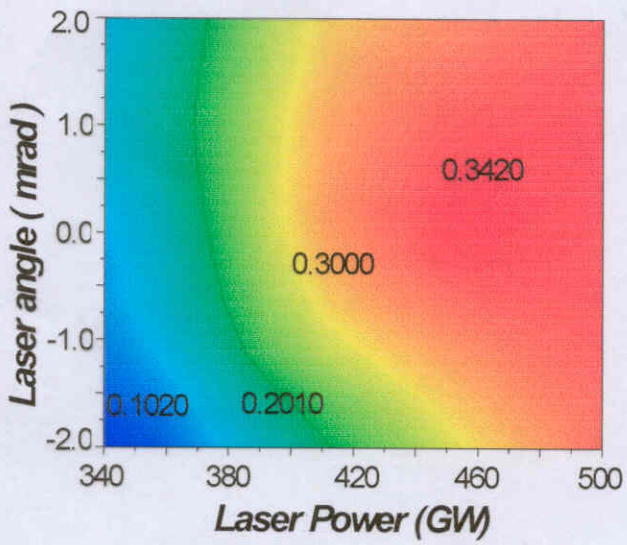

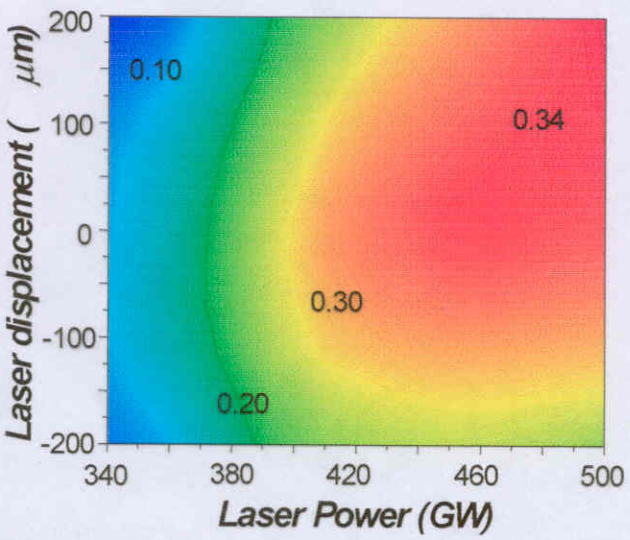

Fraction > 20% is within acceptable limits.

Laser power 0.35 ÷ 0.5 TW.

Initial energy γ 28.5 ÷ 29.0

Laser angle – 0.001 ÷ 0.001.

Laser displacement – 0.2 ÷ 0.2 m

Output beam from IFEL accelerator

Energy	55 MeV
Energy spread	2.5%
Pulse length	3 fs
Peak current	3 kA
Transverse emittance	10 mm·mrad
Trapped fraction	> 20%

Conclusion

- Vacuum laser acceleration is potential for high rate acceleration in wide energy range of accelerated particles
- Presently achievable beam qualities are sufficient for the experiment to be done on next generation on laser acceleration including first of all
  - Acceleration of electron beams up to total energy gain >100 Mev with captured fraction of beam bunch some tens % %
  - Development of staging systems with efficient prebunching providing increased beam trapping for acceleration as well as higher total energy gain due to multistage acceleration

Transverse beam bunching by laser field

- Schematic of transverse prebuncher

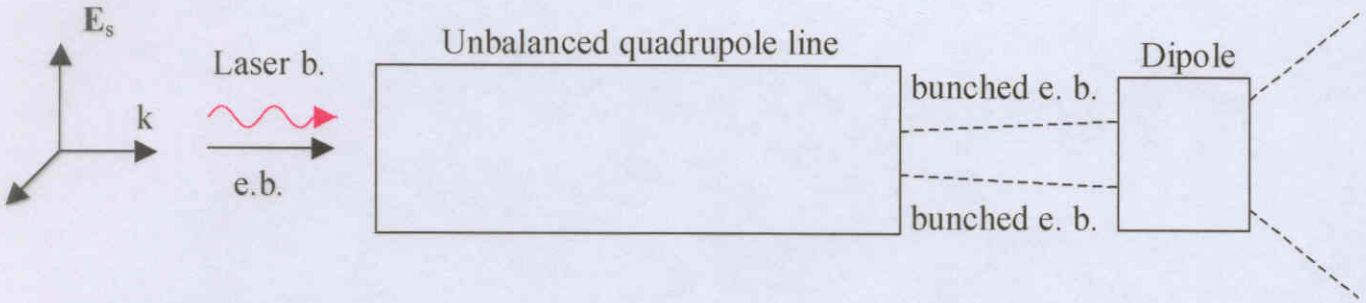

- Geometry of the fields of laser and unbalanced quadrupole causing transverse bunching.

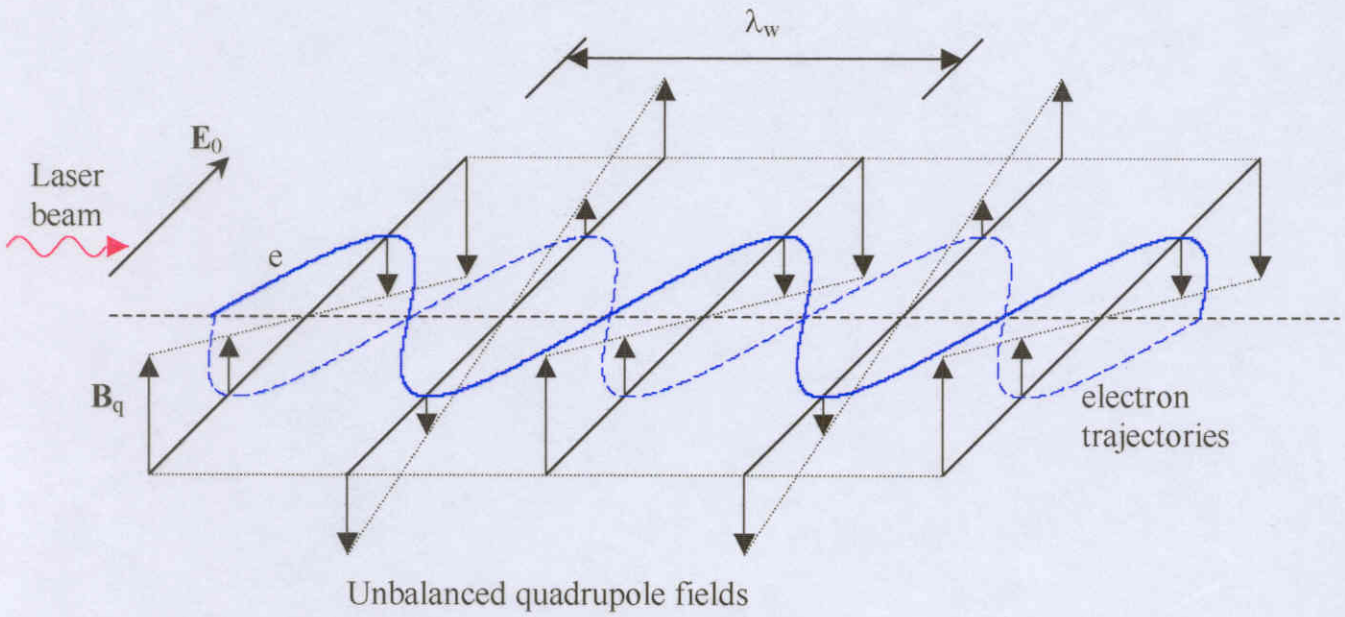

- Simulation of transverse deviations for beam bunching

P=0.7 TW,	$E_0=7\cdot10^9$ V/m,
w_0=1.8 mm,	λ_w=32 mm,
γ_0=39,	$\Delta B_q/B_q$=14%,
$r_{\perp 0}$=0; ±0.1 mm,	φ_0=0; π

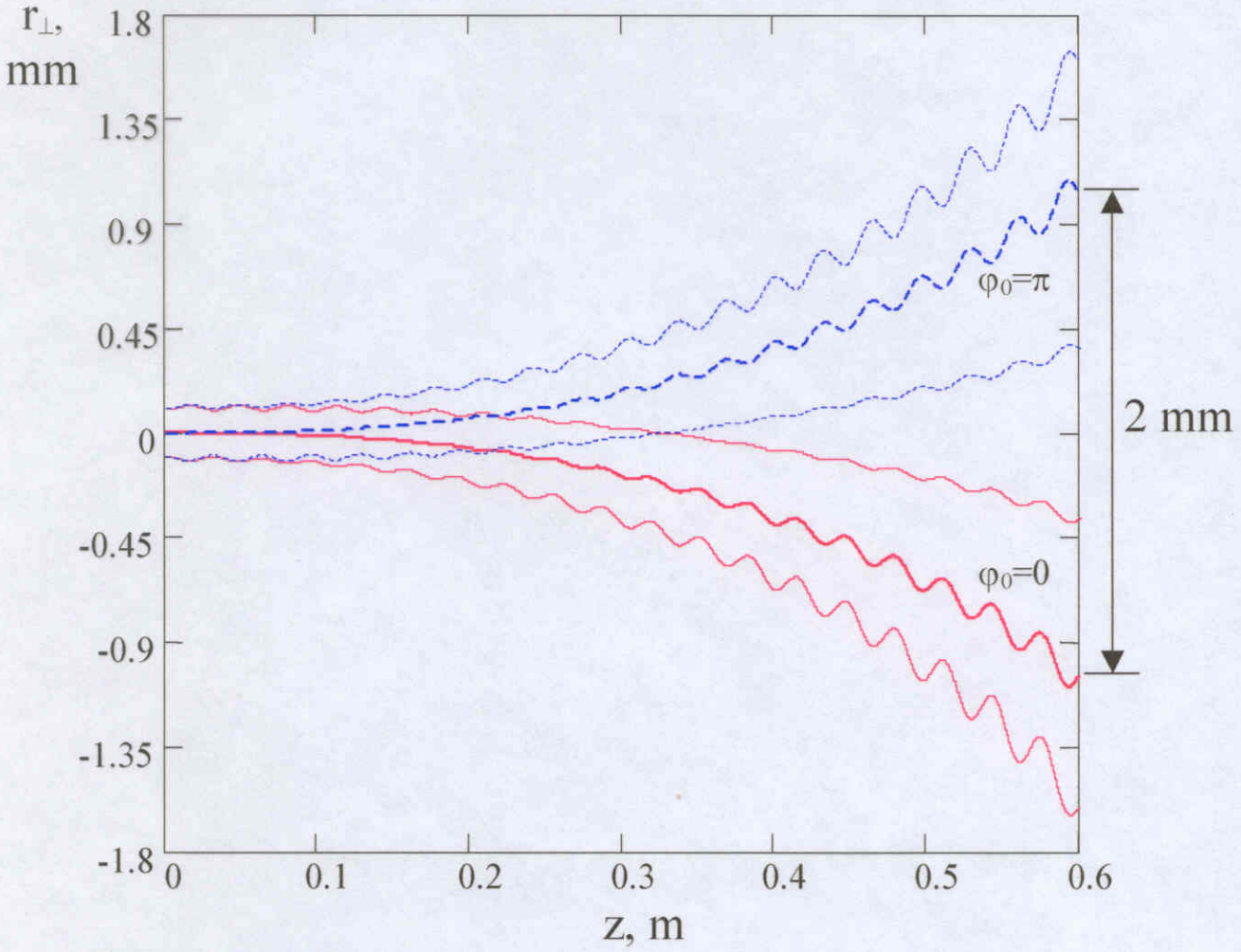

Prebunched beams separation is 2 mm
Acceptable emittance ε_n<10 mm mrad
energy spread $\Delta\gamma/\gamma$ < 1.5%

Debuncher principle scheme based on transverse bunching

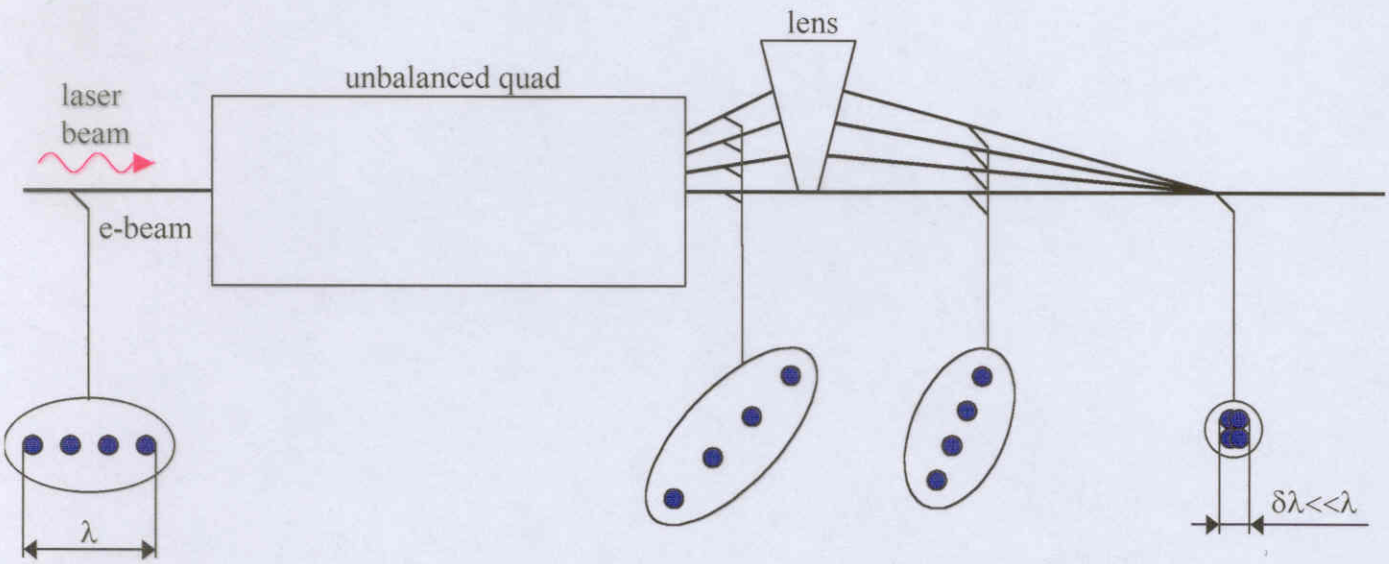

Beam density structure

Initial

Transversally bunched at an angle of deviation

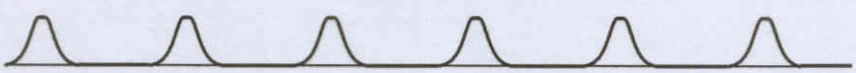

Transversally bunched and focused from all deviation angles